Exploring the novel environmentally friendly dye degradation mechanism of NiO-Polypyrrole polymer nanocomposites in degrading the organic pollutants under sunlight

Arul Raja R.A[1*] and Bhanodaya Reddy G[2]

[1]Assistant Professor (SG), Department of Mechanical Engineering, SRM Institute of Science & Technology, Vadapalani, Chennai, Tamil Nadu, India.

[2]Professor, Department of Mechanical Engineering, Sri Venkateswara University, Tirupati, Andhra Pradesh, India.

*to whom all correspondence should be addressed: raarulraja@gmail.com

Graphical Abstract

Abstract

According to estimates, around 15-50% of textile dyes fail to adhere to the fabric during the dyeing process, resulting their discharge into wastewater. This wastewater is often used for agricultural irrigation in impoverished nations which harms plant germination and development. In this study, polymer composites of Polypyrrole (PPy) and nickel oxide (NiO) nanocomposites were synthesized via the hydrothermal method with different concentrations (250 mg, 500 mg, and 750 mg) and their composite samples were employed as catalysts to degrade the anionic-brilliant blue and the cationic-crystal violet dye under 120 mins of sunlight irradiation. The process of degrading BB and CV dyes utilising nano catalysis was analysed using a pseudo-first-order kinetics model and the findings indicate that the degradation of the anionic dye is more efficient than that of the cationic dye under exposure to sunlight. Hence, the presence of NiO NPs and the NiO-PPy nanocomposite significantly impact their photocatalytic activity in degrading BB and CV dyes, achieving an impressive efficiency of around 96.99% and 89.96% respectively.

Keywords: Dye degradation, Hydrothermal, Nanocomposite, NiO nanoparticle, Polypyrrole

1. Introduction

Recent years have seen tremendous development in material science, which has brought several cutting-edge technologies to the domain of engineering. A lot of materials have become a lot more versatile in the previous hundred years (Deng *et al,* 2024). Consequently, there has been a growing demand to optimize these materials' mechanical, chemical, physical, optical, and electrical characteristics where the priority has been given to many useful materials that possess a combination of characteristics. Inorganic nanocrystalline materials attracted considerable interest because of their potential applications and scientific implications. The nanoscale dimensions of these materials give them a range of physical and chemical characteristics. Likewise, textile dyes possess toxic, mutagenic, and carcinogenic properties, rendering them potential pollutants that might infiltrate food chains (Aldhaher *et al,* 2024). Consequently, species occupying higher trophic levels are more susceptible to contamination compared to those residing at lower trophic levels. According to estimates, around 15-50% of textile dyes fail to adhere to the fabric during the dyeing process, resulting in their discharge into wastewater (Bin *et al,* 2024). This wastewater is often used for agricultural irrigation in impoverished nations. Using these dye chemicals in the soil harms plant germination and development. Recently, there has been a growing interest in conducting polymers owing to their environmentally favorable properties, durability, and redox characteristics. These attributes make them viable options for dye degradation and catalytic features. Numerous conducting polymers have garnered significant interest in the field of nanotechnology owing to their unique and remarkable characteristics. The aforementioned attributes include electrical properties, a method for conducting, a reversible doping/undoping approach, adjustable chemical and electrochemical properties, and simplicity of processing (Bones *et al,* 2020). Polypyrrole (PPy) is one of the vital heterocyclic conducting polymers for of its environmental stability and easy synthesis, exceptional physical and electrical characteristics, and cost-effectiveness. It is a conjugated polymer with absorption properties in the visible range of the electromagnetic spectrum and it facilitates the separation and transfer of charge carriers generated upon light absorption. Photodegradation of the polymer may lead to a loss of structural integrity and a decrease in its ability to facilitate charge transfer. Consequently, these limitations pose challenges in the context of catalyst applications. Possible methods to address the challenges, we can utilize the PPy as copolymers, composites, nanocomposites, or bilayers (Deng *et al,* 2024).

As a result of their fascinating physiochemical properties and attractive potential applications in many sectors, conducting polymers and hybrid nanocomposites have recently attracted a great deal of attention from academic researchers. It is expected that the characteristics of the organic polymer matrix will vary rapidly since the inorganic components have a high surface-to-volume ratio. Nevertheless, the incorporation of metal oxides by doping is an efficient way to enhance the characteristics of these materials and attain novel, unattainable outcomes through precise regulation of the dopant's passage into the polymer matrix (Du *et al,* 2020). The Nickel oxide (NiO) is a significant p-type semiconducting metal-oxide with extensive applications in conducting electrodes, sensors, catalysts, and optoelectronic devices and it is

used as a highly effective reinforcing material in preparing polymer nanocomposites due to its distinct structure and characteristics. Furthermore, the presence of Ni^{+} and Ni^{++} on the surface of the metal-oxide improves the movement of charge carriers through the CP nanocomposite by facilitating hopping and tunnelling. Thus, NiO-PPy nanocomposites offer enhanced photocatalytic activity for pollutant degradation and solar energy conversion applications compared to individual components owing to their synergetic effects between NiO nanoparticles and PPy (Duan *et al,* 2022). It also enhances light absorption, promotes charge separation, and facilitates electron transfer, leading to improved efficiency in photocatalytic reactions. The NiO-PPy nanocomposites hold promise for addressing environmental challenges, such as water purification and renewable energy generation through sustainable photocatalytic technologies. This synergistic combination harnesses the unique characteristics of both materials, offering improved conductivity, stability, and catalytic activity (Idumah *et al,* 2021.

Thus, the photocatalytic performance of materials is of paramount importance in several industrial and environmental applications. Recognizing the potential of NiO-PPy nanocomposites, we have directed the focus toward evaluating the efficacy in these domains. By harnessing the inherent properties of green synthesized NiO and the conductivity of PPy, these nanocomposites exhibit remarkable photocatalytic efficiency, paving the way for their utilization in wastewater treatment systems. In this study, we investigate the bio-synthesis of NiO using eucalyptus leaf extracts and the subsequent synthesis of NiO-PPy nanocomposites. Furthermore, we explore the photocatalytic applications of the prepared nanocomposites.

2. Experimental procedure

2.1. Materials and Methods

Reagents used were obtained from Merck and were purified to an analytical grade before use. Nickel nitrate [$Ni(NO_3)_2$], Double Distilled water (DD H_2O), Ethanol (C_2H_5OH) (99.9%), Polypyrrole ($H(C_4H_2NH)_nH$) were procured from Isochem Laboratories, India.

2.2 NiO nanoparticle synthesis using E. leaf Extract

Initially, the leaves of *Eucalyptus teriticornis* were washed with refined distilled water to get rid of any undesired contaminants and suspended particles. Then, they were dried in light shade and subsequently processed into a fine powder using a home blender. A quantity of 5 g of powder was combined with 200 ml of distilled water and agitated at 70℃ for 30 minutes. Subsequently, the extracts were allowed to cool to the ambient temperature and then subjected to filtration through Whatman filter paper. The nickel oxide nanoparticles were synthesized by gradually combining a 0.2 M solution of nickel nitrate with 100 ml of extracts using a magnetic stirrer which was maintained continuously for 24 hours. At 80°C, the solution is placed under sonication for 35 min. The particles were centrifugated at 6000 rpm for 20 min and it is rinsed with distilled water and ethanol to eliminate undesired contaminants. Finally, a powder of nickel oxide nanoparticles was obtained by drying the purified precipitant at 500°C in a Muffle furnace for 4 hours, forming nickel oxide nanoparticles (Khattab *et al,* 2020).

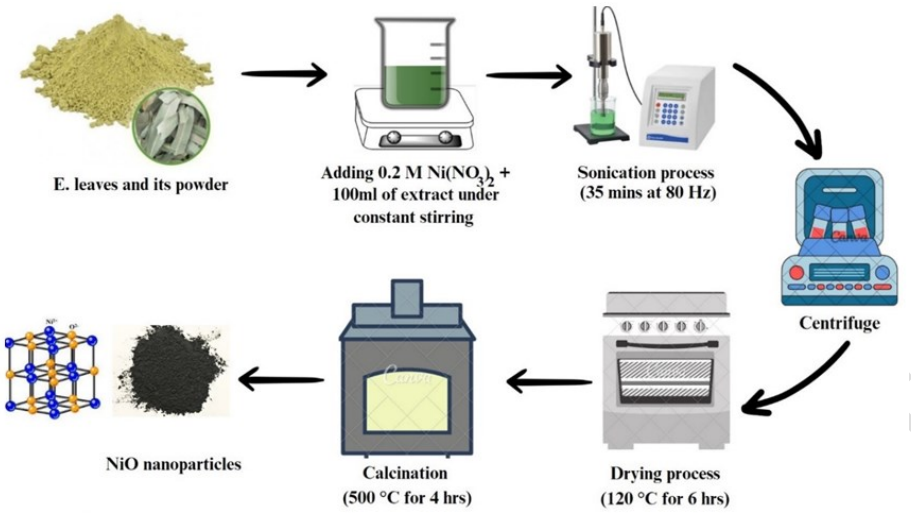

Figure 1. Schematic illustration of NiO nanoparticles synthesis

2.3 Preparation of nanocomposite materials

The nanocomposites with three distinct concentrations were synthesized using hydrothermal treatment. A certain amount of 1 gram of NiO nanoparticles was combined with 250 mg of Polypyrrole polymer, followed by a further 30 minutes of vigorous agitation and the samples were placed in a stainless-steel autoclave coated with Teflon. The autoclave was then sealed, heated to a temperature of 180°C for 12 hours, then cooled gradually. Before drying in an oven at 60°C overnight, the reactants underwent centrifugation and were rinsed many times with deionized water and ethanol. Once the Polypyrrole nanocomposites were dried, they were subjected to calcination in a muffle furnace for two hours at 200°C and the material has been referred to as NiO-P_1. In addition, the same method is applied to nanocomposites with concentrations of 500mg and 750 mg, which are referred to as NiO-P_2 and NiO-P_3, respectively.

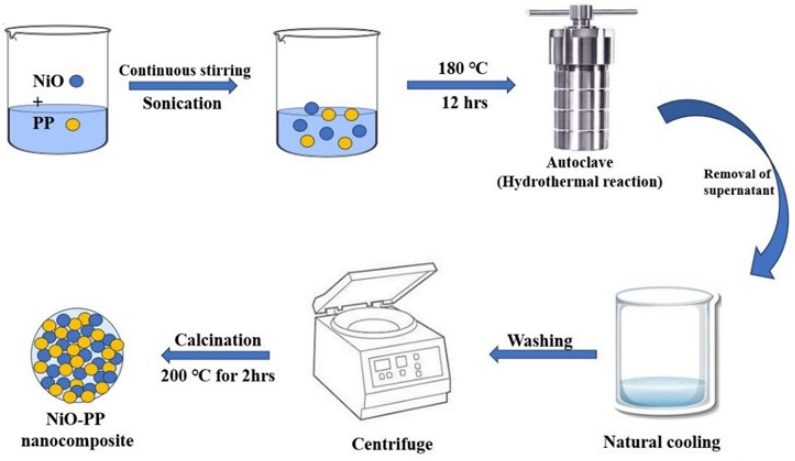

Figure 2. Schematic representation of nanocomposite synthesis

2.4. Photocatalytic degradation

The synthesized NiO nanoparticles and NiO-PPy nanocomposite demonstrated photocatalytic activity by degrading anionic Brilliant blue dye and cationic Crystal violet dye when exposed

to sunlight irradiation. Optimal degradation efficiency within a certain time frame was initially achieved by optimizing the initial concentration of the dye solution. Next, the nano-suspension solution was made by adding, one by one, 0.5 g/L of nano-catalyst and 5 mg/L of dye solutions to a room-temperature solution. The mixture was agitated in darkness for 30 minutes to achieve equilibrium before being exposed to sunshine. After every 15 minutes of irradiation, 3 ml of the solution combination was taken out and analyzed using UV-Vis spectroscopy in the 200-800 nm wavelength range to assess the dye degradation. The treatment was maintained until it was completely degraded. The equation (1) below can determine the degradation efficiency using a nano catalyst Where C_t and C_0 are the final and initial concentrations of dyes, respectively (Liu *et al,* 2022).

$$\text{Degradation Efficiency (\%)} = 1 - \frac{Ct}{Co} \times 100\% \quad (1)$$

2.5. Characterization techniques

A comprehensive examination was conducted on the physicochemical properties of NiO and NiO-PPy nanocomposite synthesized through green synthesis, employing the following methodologies. The structural and phase purity features were scrutinized using XED where the sample was scanned with a step size of 0.02 within 10- 80° at apartment temperature. The functional group and infrared spectra of the material were determined using FTIR during transmission or absorption. We used a pestle and mortar to pulverize the sample and KBr (1:200 ratio) before processing it into pellets through a hydraulic pellet machine (Perkin Elmer, Mumbai, India). Nanophox, made by Sympatec in Germany, was used to calculate the mean distribution of particle sizes. Using a scattering angle of 90°, DLS was used in the 1-100 nm range. The surface topography and flaws were examined using FE-SEM and the microscope utilised was the SIGMA HV Carl Zeiss. The UV-Vis spectrophotometer was utilized to measure the absorption spectra of NiO and nanocomposite in the wavelength of 200-800 nm (Cary 8454; Agilent, Singapore).

3. Results and Discussion

3.1. Crystallinity and Phase purity analysis

The XRD pattern was utilized to inspect the structural characteristics and crystallinity of NiO NPs synthesized using E. leaf extract. The XRD pattern presented in Figure 3 depicts the diffraction pattern of NiO powder derived from the decomposition of the precursor calcinated at 500°C. Five distinct Bragg peaks are prominently observed, with their peaks positioned at 2θ angles of 37.2°, 43.2°, 62.8°, 75.4°, and 79.2°. These observed diffraction peaks correspond to the crystallographic planes (1 1 1), (2 0 0), (2 2 0), (3 1 1), and (2 2 2), respectively which are consistently assigned to the cubic structure of NiO (indexed as per JCPDS card number= 96-101-0096) (Liu *et al,* 2022). The cubic structure fit in to the space group Fm-3/m with a space number of 225, featuring a lattice parameter of a=b=c=4.1800 Å. The absence of impurity peaks indicates the formation of highly pure NiO nanoparticles. Furthermore, the relatively broadened peaks, compared to their bulk counterparts, suggest that the deposited material possesses a very small crystalline size (Lv *et al,* 2020). Meanwhile, the pronounced peak

intensities affirm the high crystallinity of NiO nanoparticles, corroborating with the findings from SEM analysis. Additionally, a broader peak observed at 2θ = 13°-21° signifies the amorphous nature of the polypyrrole polymer which is the characteristic of polypyrrole, arises from scattering from polymer chains at the interplanar spacing. Moreover, at higher concentrations, polymer chains have a higher probability of aligning in a preferred orientation and this may be the reason for the increase in polymer intensity observed in XRD when concentration is increased. The average microstrain was measured to be 0.3813% and crystal size (D) was measured to be 21.72, 22.5, 23.62, and 24.2 nm respectively for the NiO, NiO-P_1, NiO-P_2, and NiO-P_3 calculated using the Debye–Scherrer formula (Pandey *et al,* 2021). Moreover, XRD measurement confirmed the presence of Polypyrrole polymer in the NiO-PPy nanocomposites.

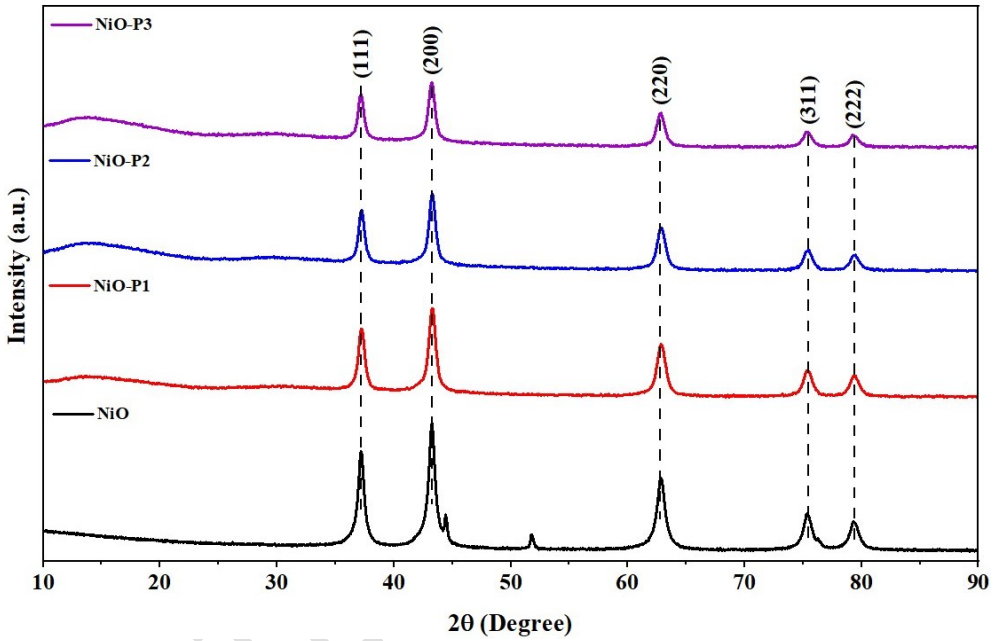

Figure 3. XRD spectra of prepared NiO NPs and nanocomposite

3.2. Functional group analysis

To identify the functional groups, present in a prepared sample based on the absorption of infrared radiation, FTIR spectra are used and the corresponding bands and functional groups are displayed in Figure 4. The 3414 cm^{-1} peak agrees to the stretching vibration of O-H bonds, representing the presence of hydroxyl groups (Peng *et al,* 2024). In green synthesis methods, these hydroxyl groups might originate from the capping agents or stabilizers used during the synthesis process, such as plant extracts or biomolecules. The minor peak at 2918 and 2848 cm^{-1} is allied with the asymmetric stretching vibrations of C-H bonds in aliphatic compounds (Restrepo *et al,* 2021). The band at 1734 cm^{-1} specifies the stretching vibrations of C=O bonds, implying the presence of carbonyl groups resulting from surface adsorbed carbon dioxide or moisture. The wavenumber at 1365 cm^{-1} can be recognised to the stretching vibrations of C-N bonds in polypyrrole (Tian *et al,* 2024). It is characteristic of the pyrrole ring structure in polypyrrole. These results indicate that polypyrrole has been formed. The peak at 1629 cm^{-1} is typically related with the stretching vibrations of C=C bonds, representing the presence of unsaturated hydrocarbons or aromatic compounds (Walkinshaw *et al,* 2020).

The bending and stretching vibrations of Ni-O bonds at 1469-1054 cm^{-1} further confirm the presence of NiO NPs in the prepared sample and the broad peak range at 887-400 cm^{-1} is typical for metal oxides. It represents the stretching vibrations of metal-oxygen (Ni-O) bonds, confirming the presence of NiO NPs in the nanocomposite. In the case of nanocomposites, as the concentration of Polypyrrole polymer increases, there could be a tendency for agglomeration of nanoparticles, leading to a decrease in the surface area available for interaction with infrared radiation or distribution of nanoparticles within the polymer matrix which can result in a reduction in the intensity of FTIR peaks (Yan *et al,* 2021).

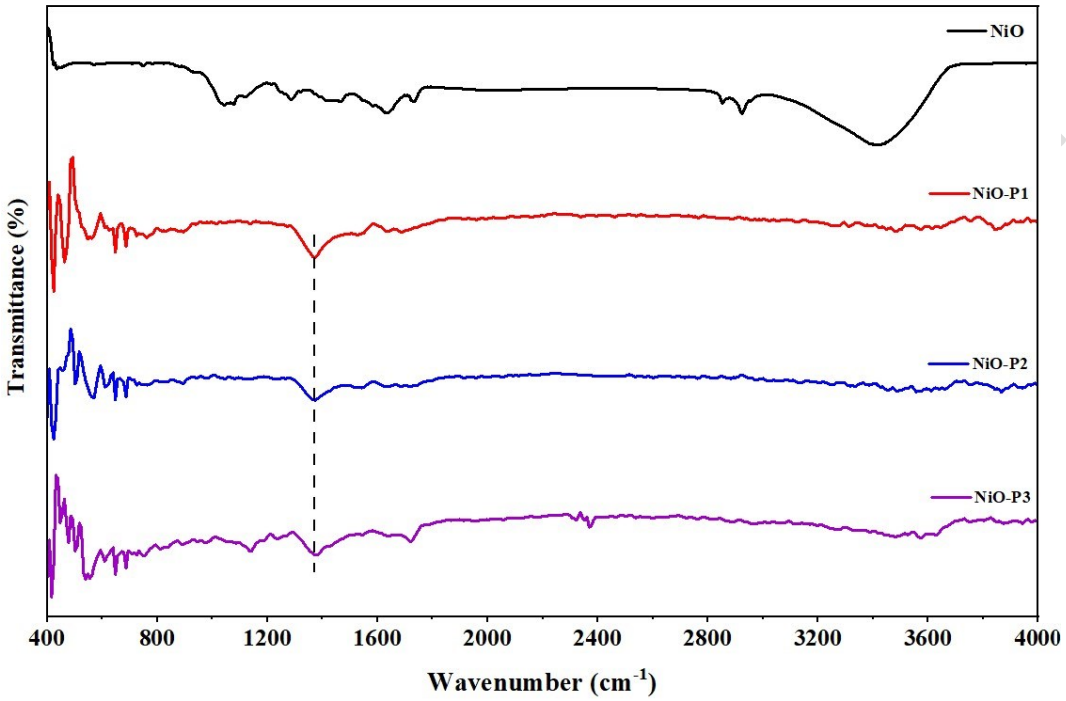

Figure 4. FTIR analysis for the prepared NiO NPs and nanocomposite

3.3. Particle size analysis (PSA)

The Particle Size Analysis results insights the size distribution of the NiO NPs and NiO-PPy nanocomposite as represented in Figure 5. The PSA result indicates that the mean particle size of NiO nanoparticles is approximately 35.34 nm.

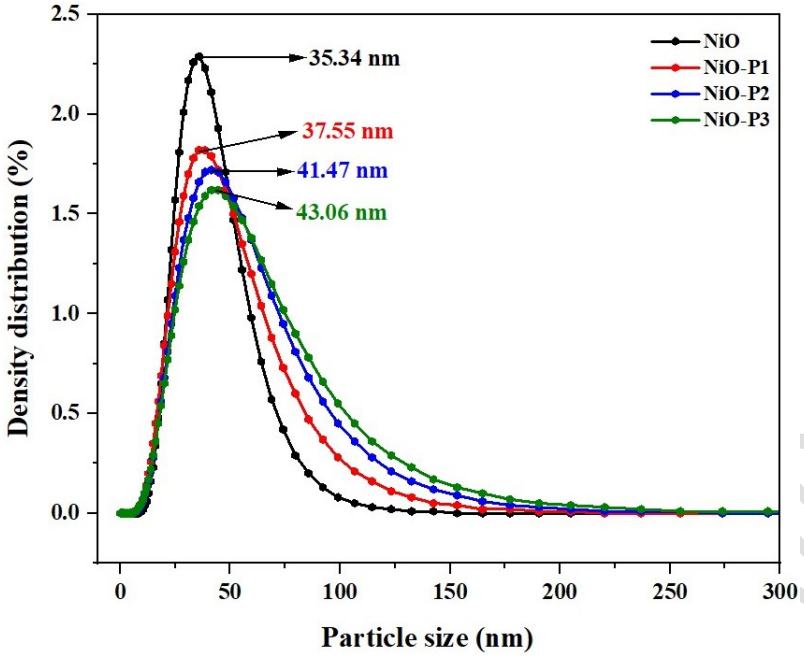

Figure 5. PSA image of prepared NPs and nanocomposite

The presence of stabilizing agents or surfactants in the synthesis process can influence the growth and aggregation of nanoparticles, leading to a specific particle size distribution (Yan *et al,* 2021). For NiO-PPy nanocomposites, it shows an increase in average particle size compared to pure NiO nanoparticles. The incorporation of polypyrrole polymer into the nanocomposite can increase the overall size of the particles. Polypyrrole layers or coatings around the NiO nanoparticles can contribute to the observed increase in size as demonstrated in the SEM images.

3.4. UV-Visible spectroscopy

The Figure 6 shows the optical characteristics of the prepared nanoparticles and NiO-PPy nanocomposite. In the UV-visible spectrum of NiO nanoparticles, you would typically observe absorption peaks in the UV region, with a characteristic peak around 320 nm. When NiO nanoparticles are incorporated into a composite material (NiO-PPy), the UV-visible spectrum exhibits changes compared to pure NiO nanoparticles. As the concentration of the composite material increases, a decrease in the intensity of the absorption peak is observed. At higher concentrations of the composite (NiO-P_3), the scattering and absorption of light by the polymer matrix become more pronounced (Zhao *et al,* 2024). This can result in a reduction in the observed intensity of the NiO absorption peak. The bandgap of NiO NPs is approximately 3.5 eV. Thus, NiO is in the category of wide-bandgap semiconductors which exhibits an indirect bandgap, this characteristic influences the optical and electronic properties of NiO NPs. Due to its wide bandgap, NiO is typically transparent in the visible range of the electromagnetic spectrum and absorbs light in the ultraviolet (UV) region (Zheng *et al,* 2022). Table 1 shows the crystal and particle size values for the prepared samples.

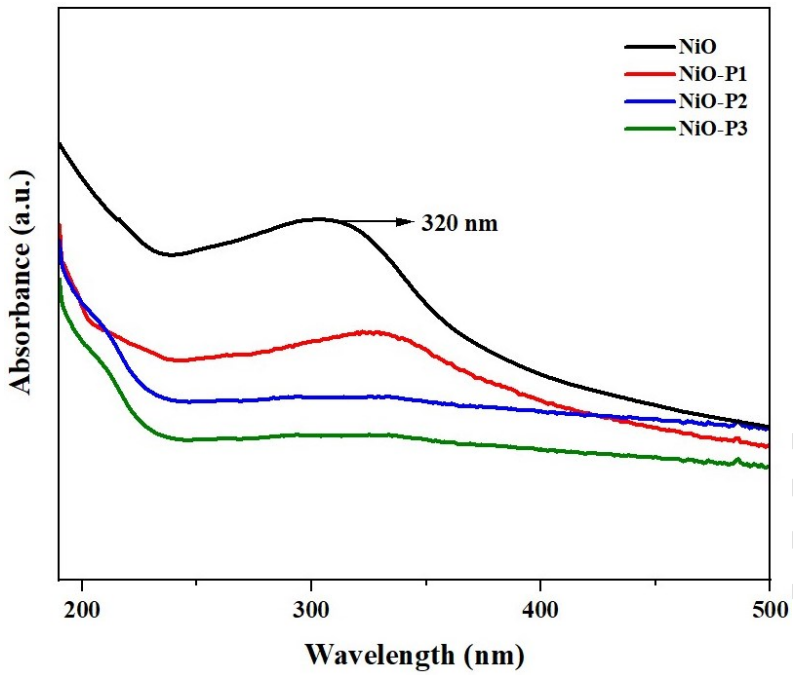

Figure 6. UV -Visible spectra of prepared NiO NPs and nanocomposite

A typical FE-SEM image of green-synthesized nanoparticles and NiO-PPy nanocomposite is portrayed in Figure 7, which reveals the formation of nanoflakes morphology. For pure NiO NPs, shows spherical morphology with agglomeration. For nanocomposites, the growth of nanoflakes can be influenced by the anisotropic nature of crystal growth.

Table 1. Crystal and its particle size values for the prepared samples

Sample	Particle size (nm)	Crystal size (nm)	Bandgap (eV)
NiO	35.34	21.72	3.57
NiO-P1	37.55	22.5	3.55
NiO-P2	41.47	23.62	3.53
NiO-P3	43.06	24.22	3.52

3.5. Morphology Analysis (FE-SEM)

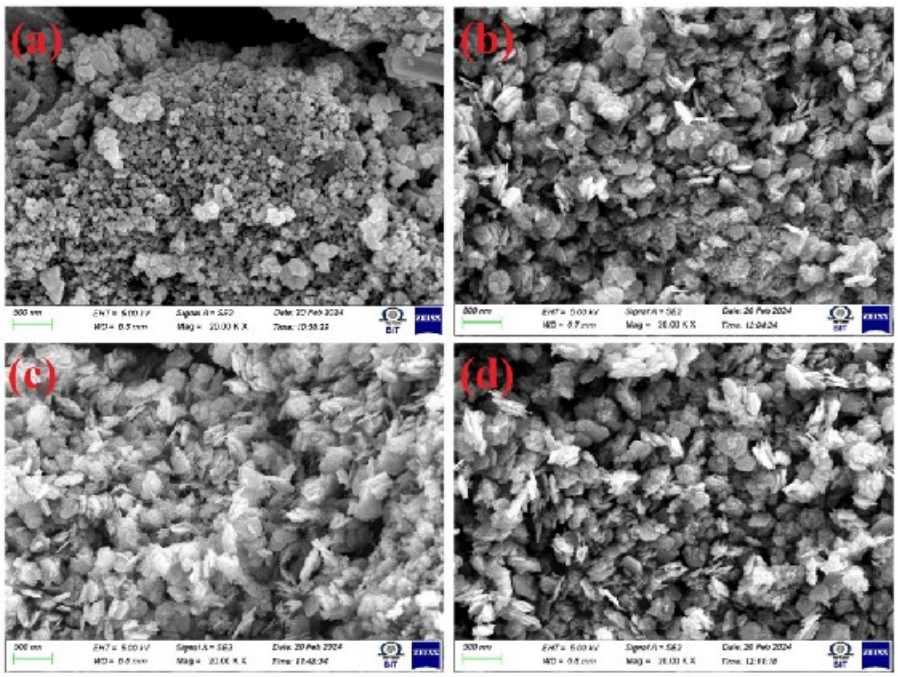

Figure 7. FE-SEM of prepared nanoparticle and its composite

This anisotropy can lead to preferential growth along specific crystal planes, resulting in the formation of nanoflakes with a plate-like morphology. During the hydrothermal synthesis process, NiO nanoparticles may undergo Ostwald ripening phenomena (Walkinshaw *et al,* 2020). The nanoflake morphology in NiO and its composites can result from Ostwald ripening, while this phenomenon involves the dissolution of smaller particles and the growth of larger ones, favoring the formation of nanoflake morphology and the polypyrrole can stabilize the NiO nanoparticles and prevent their agglomeration during synthesis. This stabilization effect may contribute to the formation of well-defined nanoflakes morphology in the composite material. The Figure 8 illustrates the elemental analysis of the prepared nanoparticles and NiO-P_1, NiO-P_2, and NiO-P_3 nanocomposites. The EDX spectrum displays the existence of Nickel (Ni) and oxygen (O) and shows the high purity in the prepared NiO samples. Moreover, the composite samples (Figure 8 c, d, and e) indicate some organic components present in the eucalyptus leaf extract could result in a decreased weight percent of carbon (C) content.

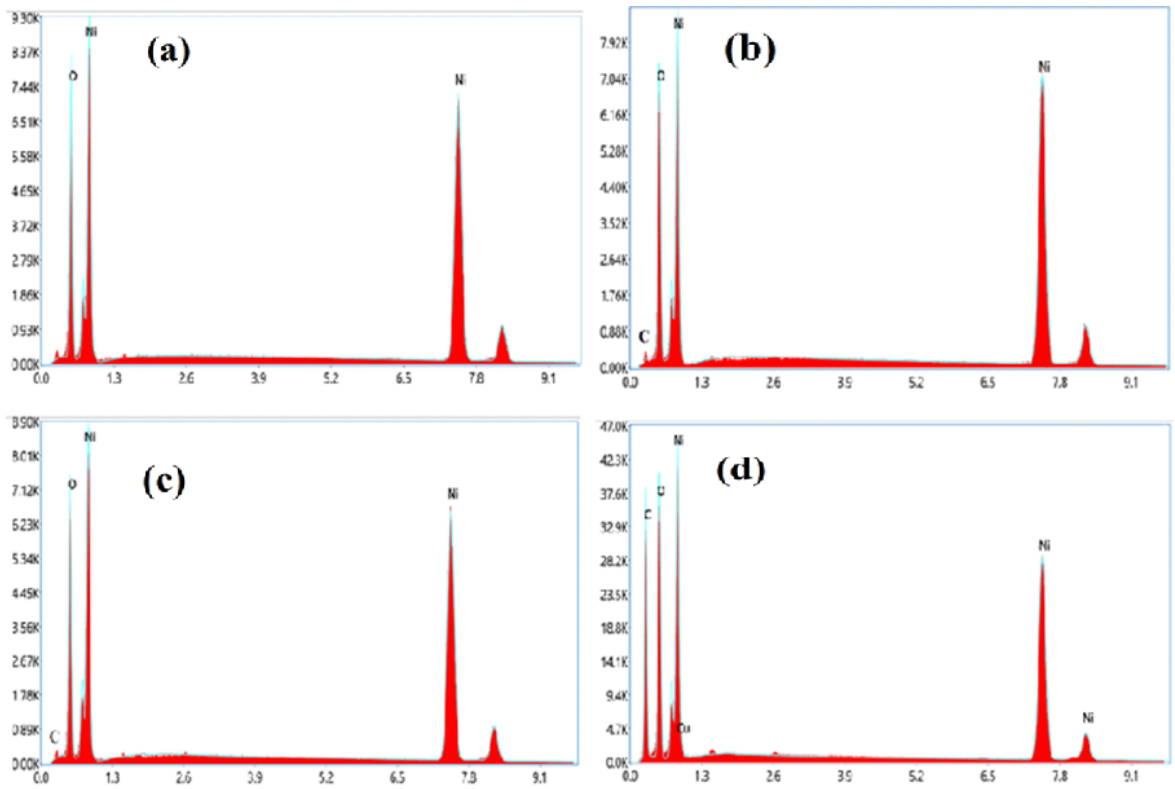

Figure 8. EDX picture of nanocomposite and prepared NPs

Elemental mapping is an imaging technique used to identify the distribution of different elements within the prepared nanocomposite. Here, from Figure 9 shows the distribution of nickel (Ni), oxygen (O), and carbon (C) within the composite material. The Figure 9 (a) represents the grey image and (b) corresponds to the element being mapped and the weight percent of the elements in the sample area. The image (c, d, e, f) shows that the nickel (blue) is uniformly distributed throughout the composite material. The oxygen (pink) is also distributed throughout the composite material, but it is more concentrated in some areas than others. The carbon (green) is mostly concentrated in the background, which is likely to be the polymer matrix.

3.6. Photocatalytic activity

Due to the desirable band alignment of bio-synthesized NiO and NiO-PPy nanocomposites, we conducted a study on the photocatalytic activity of the prepared nanocatalyst. Our focus was on the degradation of anionic brilliant blue (BB) dye and cationic crystal violet (CV) dye under sunlight irradiation. Figures 10 and 11 show time-dependent absorption spectra of the BB and CV solution during sunlight irradiation in the presence of NiO and NiO-PPy nanocomposites. UV light has the intriguing ability to create electron-hole pairs for redox reactions in NiO NPs (Khattab *et al,* 2020). This is due to the specific bandgap between the valence band and conduction band of NiO NPs, which measures 3.5 eV. As a result, UV light with a wavelength greater than 354 nm. This is because of the distinct energy difference between the valence band and conduction band of NiO nanoparticles which is precisely 3.5 eV. Consequently, UV

radiation with a wavelength above 354 nm can generate electron-hole pairs (Walkinshaw *et al,* 2020),

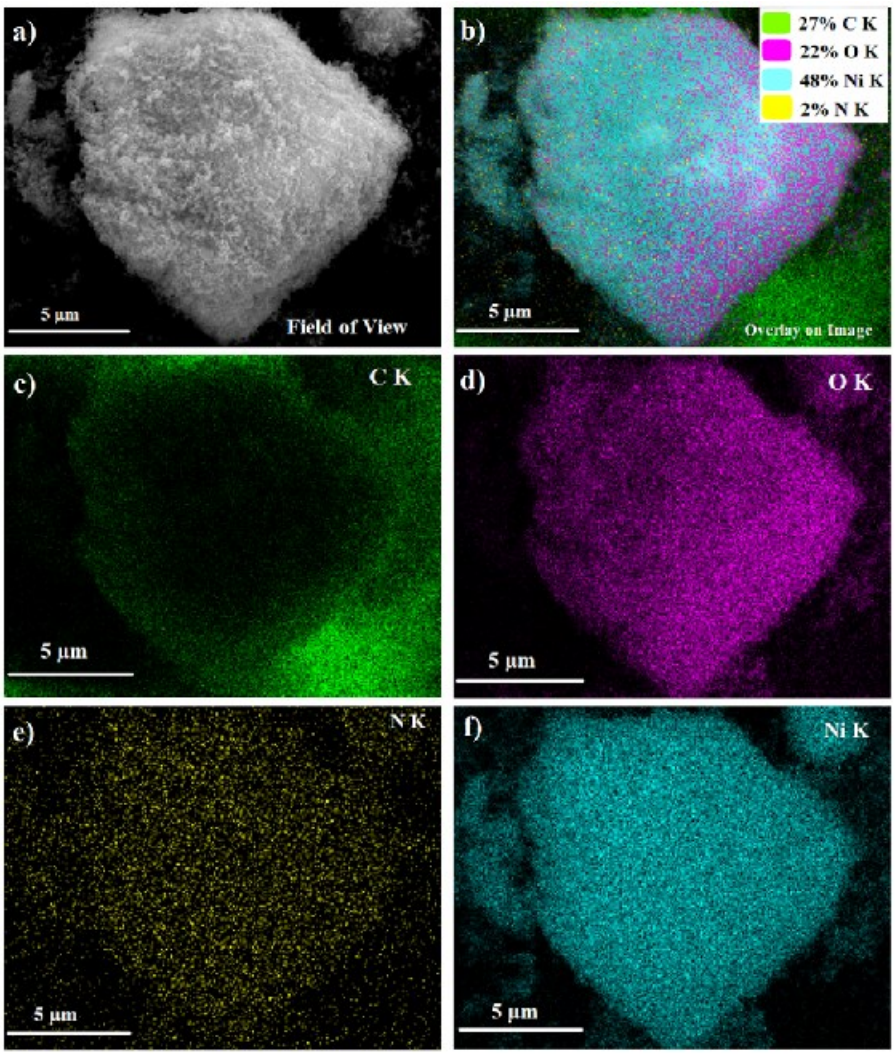

Figure 9. Elemental mapping image of prepared NiO NPs and its composite

The photocatalytic activity of bio-synthesized nanoparticles and NiO-PPy nanocomposites can be assessed by monitoring the degradation of BB dye and CV dye under sunlight irradiation. Similarly, we can measure the decrease in absorbance at the characteristic peaks of each dye (around 564 nm for BB and 590 nm for CV) at regular time intervals. A decrease in the absorbance at these peaks would indicate the breakdown of the dye molecules (Du *et al,* 2020). Additionally, the shift in the absorption peaks of the degradation products might be observed, compared to the original dyes. This shift could suggest the formation of smaller molecules with different structures (Pandey *et al,* 2021). The overall decrease in absorbance intensity with irradiation time would signify a reduction in the concentration of the dye solution, confirming the photocatalytic degradation of BB and CV dyes by NiO NPs and NiO-PPy nanocomposites.

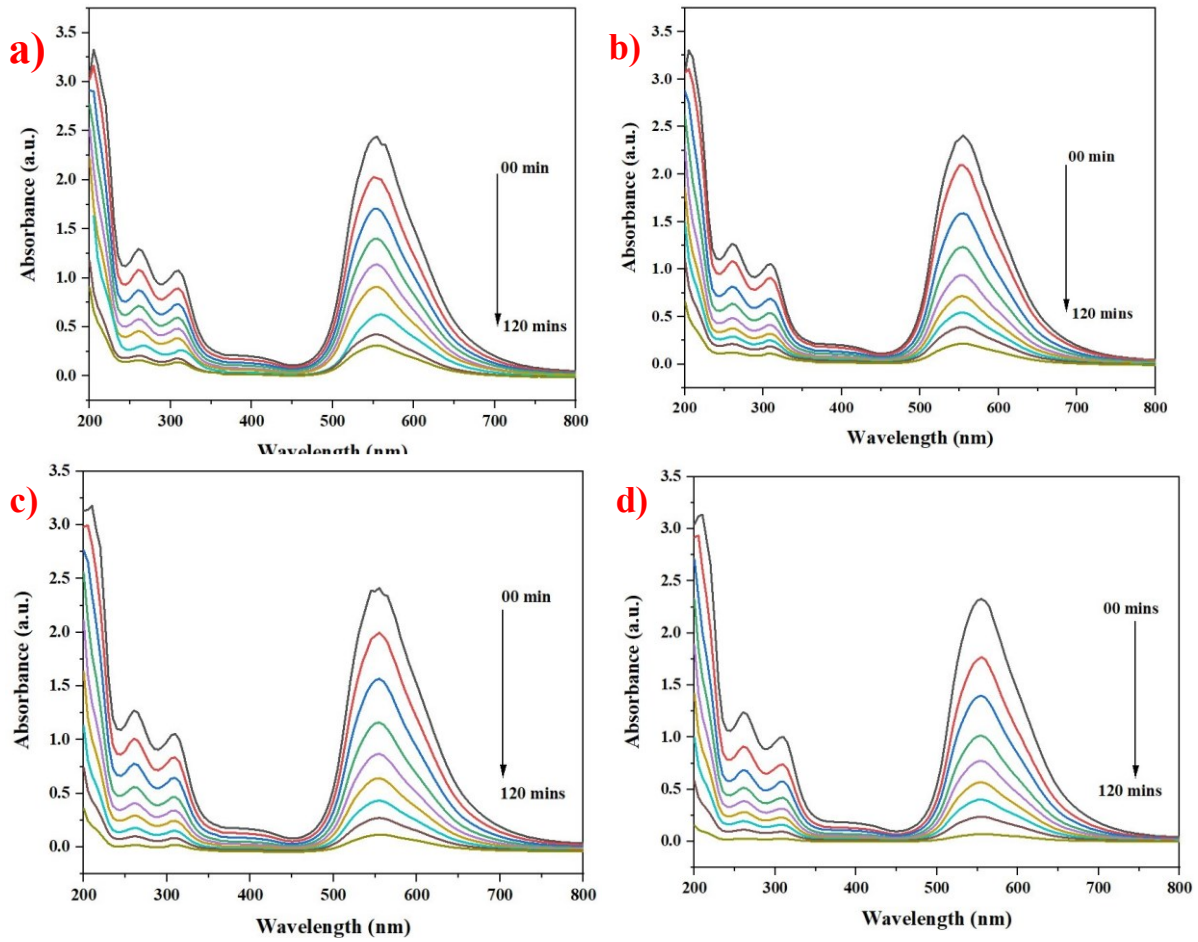

Figure 10. Time-dependent absorbance spectra of BB dye. a) NiO, b) NiO-P1, c) NiO-P2 and d) NiO-P3

The Figures 12 (c) and (d) show the degradation efficiency of the nanocatalyst and the degradation efficacy of the NiO NPs and NiO-PPy nanocomposites for BB dye was observed to be 87.2, 91, 95.1 and 96 %, respectively for NiO, NiO-P_1, NiO-P_2, and NiO-P_3 nanocomposites. Similarly, for CV dye, it is observed that 80.3, 83.1, 87.6 and 89.9 % for NiO, NiO-P_1, NiO-P_2, and NiO-P_3 nanocomposites within 120 min, and thus, BB and CV dyes were completely degraded into colourless small molecules (Yan *et al,* 2021). The Figure 13 (a) and (b) represents the plot of log(C/Co) vs time graph which implies that the degradation of the BB and CV dyes follows pseudo-first-order kinetics as explained in the following equation, and the plot of C/Co vs time graph (Figure 12 (a, b)) for the degradation of BB and CV dyes by NiO NPs and NiO-PPy nanocomposites by applying sunlight radiation, and rate constant values were tabulated in table 2. The kinetics of photocatalytic degradation rate constant are calculated using the Eq. 2 (Walkinshaw *et al,* 2020),

$$Kt = -\ln\left(\frac{C}{Co}\right)$$

Where, the reaction concentration is amplified as C/Co, concentration of dyes after degradation of time.

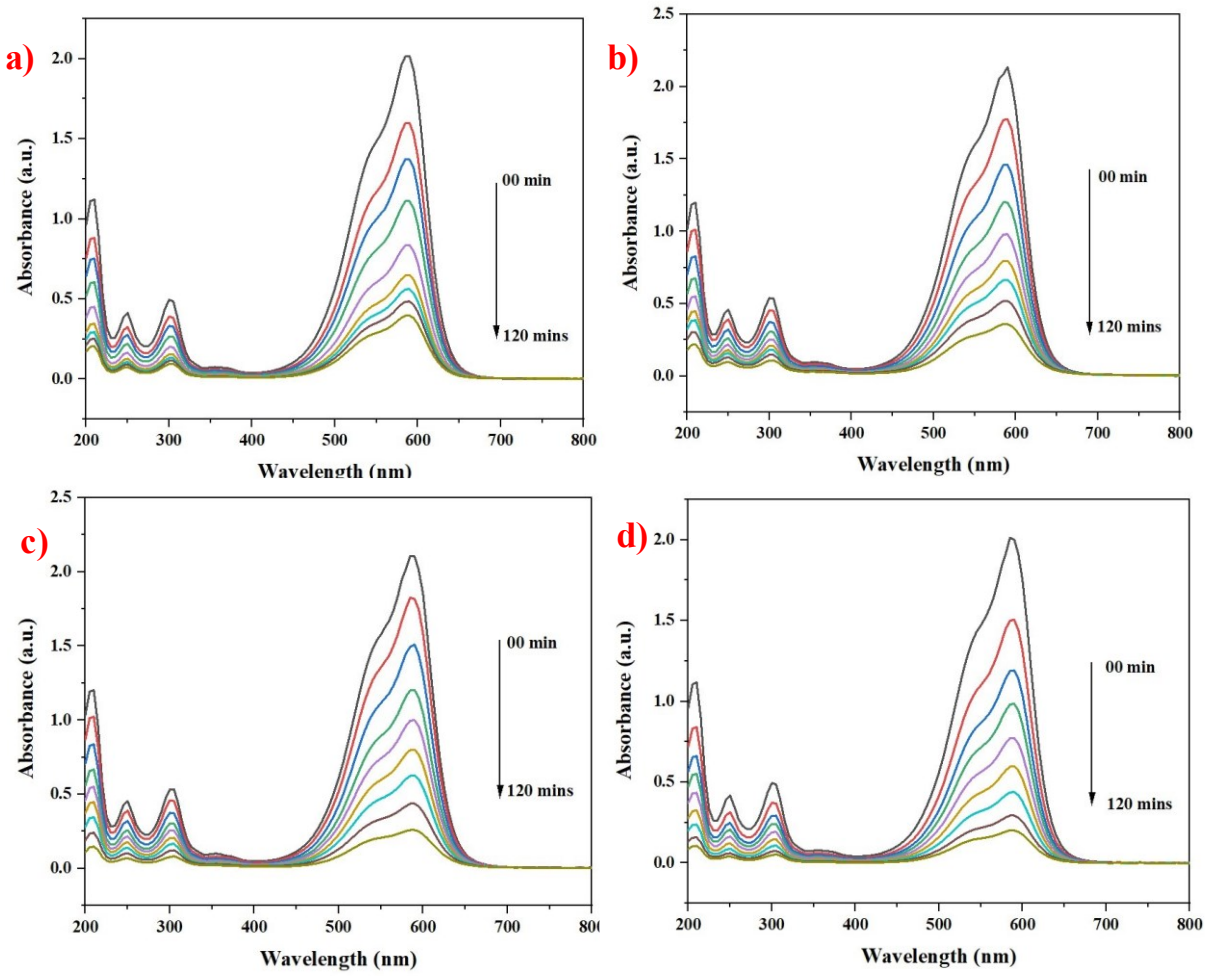

Figure 11. Time-dependent absorbance spectra of CV dye. a) NiO, b) NiO-P1, c) NiO-P2 and d) NiO-P3 nanocomposite

The findings illustrate the progressive increase in the breakdown rate of the dye when exposed to sunlight. In a similar manner, the results specify that the relative concentration (C/Co) of the dyes decreases as the irradiation-exposed time increases at different concentrations. Therefore, the polymer functions as a highly effective photocatalyst for the substantial breakdown of dyes when visible to sunlight. Moreover, Polypyrrole facilitates the separation and transfer of charge carriers generated upon light absorption when photons are absorbed by the composite material, electron-hole pairs are created. Polypyrrole provides a pathway for these charge carriers to migrate, reducing their chances of recombination. Efficient charge separation and transfer are crucial for maintaining high photocatalytic activity (Tian *et al,* 2024). Overall, nanocomposite materials show improved photocatalytic performance than the bare NiO NPs.

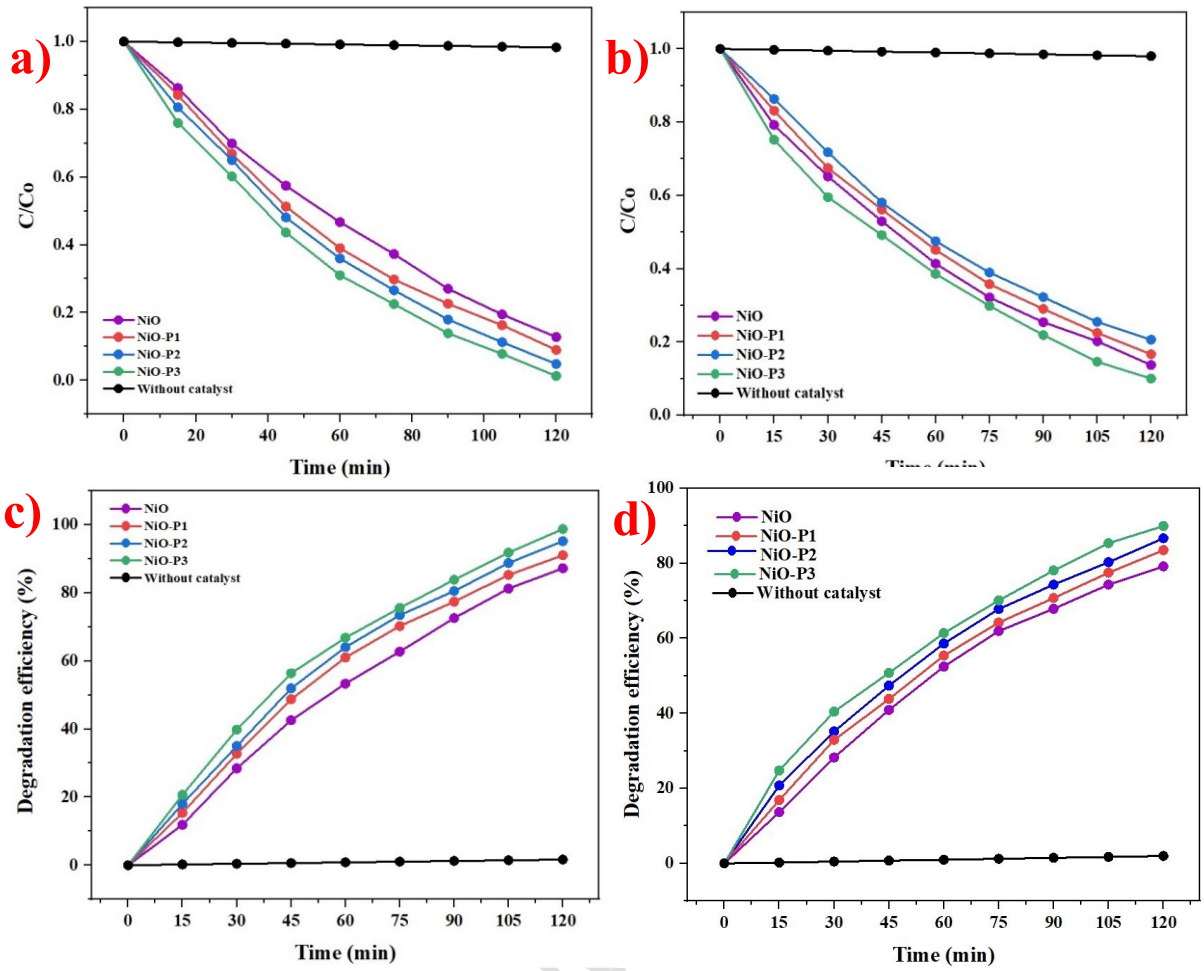

Figure 12. a) C/Co graph and c) degradation graph for BB dye and b) C/Co graph and d) degradation graph for CV dye.

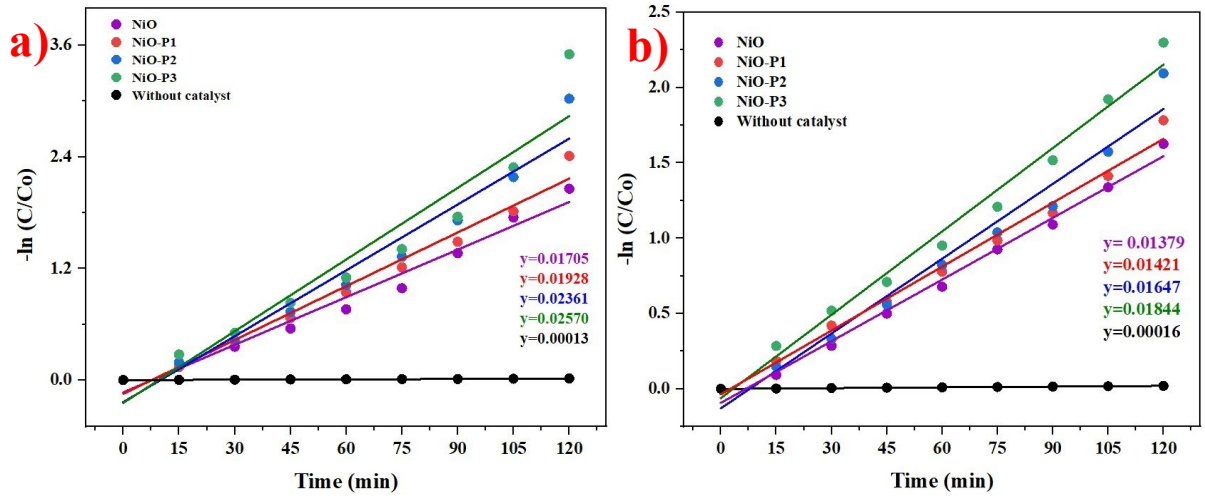

Figure 13. Pseudo-first-order kinetics graph. a) BB dye, b) CV dye for the prepared NiO NPs and nanocomposite.

Table 2. Degradation rate constant and efficiency of nanocatalysis

Sample	Pollutant used	Irradiation time	Kinetic rate constant (x10^2 min^{-1})	Degradation efficiency (%)
NiO	Brilliant blue	120 mins	1.70	87.22
NiO-P1			1.92	91.02
NiO-P2			2.36	95.15
NiO-P3			2.57	96.99
NiO	Crystal violet	120 mins	1.38	80.33
NiO-P1			1.42	83.17
NiO-P2			1.64	87.69
NiO-P3			1.84	89.96

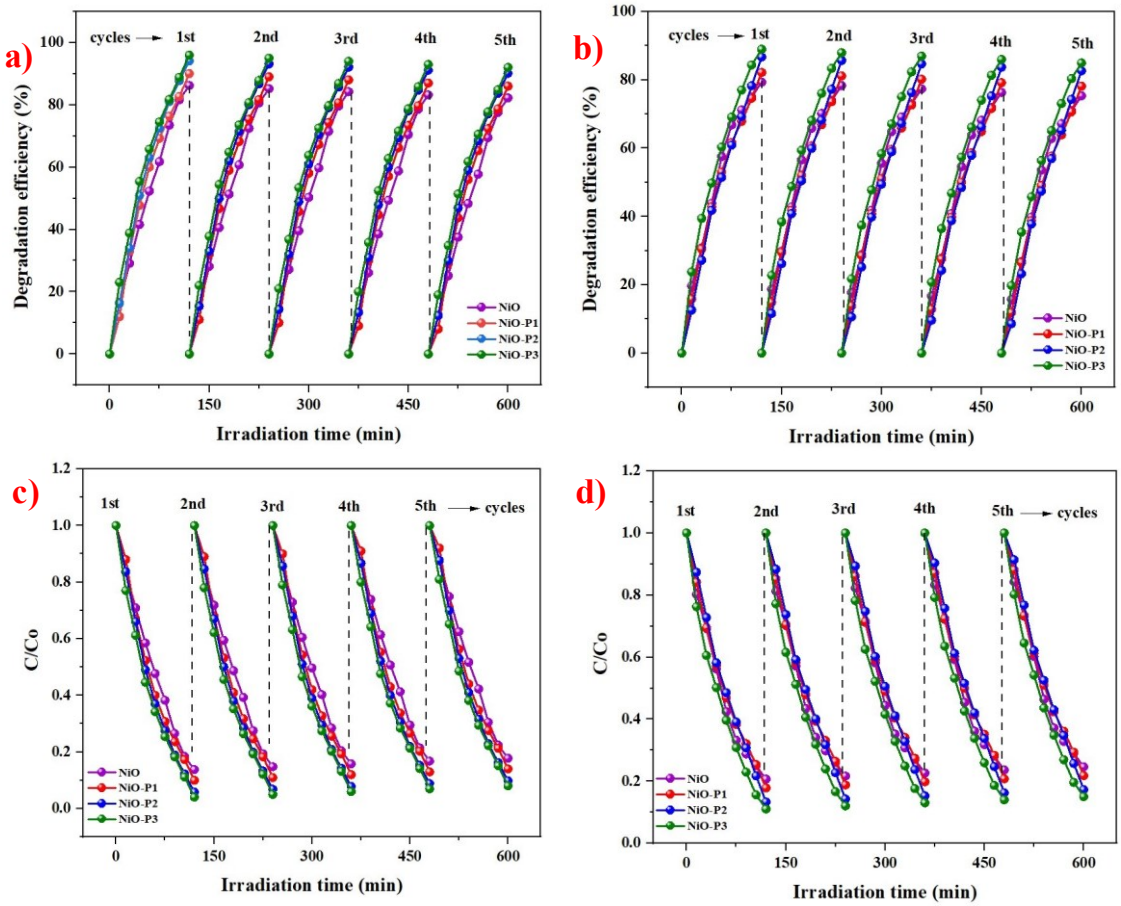

Figure 14. Recycling stability for BB dye (a, b) and CV dye (c, d)

The stability of the created NiO nanoparticles and NiO-PPy nanocomposites was assessed using recycling tests conducted under comparable conditions and the photodegradation studies were conducted five separate times using the same catalyst while being exposed to sunlight. The outcomes derived from the recycling processes are shown in Figure 14. After five successive cycles, the degradation efficiencies of anionic dye (BB dye) were 82.2%, 86%, 90.1%, and 91.9% for NiO, NiO-P_1, NiO-P_2, and NiO-P_3, respectively. Similarly, the cationic dye (CV dye) content for NiO, NiO-P_1, NiO-P_2, and NiO-P_3 nanocomposites is 75.3%, 78.1%,

82.6%, and 84.96%, appropriately. A slight reduction in the effectiveness of photodegradation was observed after every cycle. After undergoing five consecutive cycles under sunlight, the biosynthesized NiO nanoparticles and NiO-PPy nanocomposites demonstrated 91.9% and 84.96% activity levels for anionic and cationic dyes, respectively. Therefore, it can be deduced that the catalyst that has been synthesized exhibits efficacy and reusability when exposed to sunlight.

3.7. Degradation Mechanism

When NiO is exposed to light energy, such as visible light, it absorbs photons and generates electron-hole pairs. This excitation of electrons to higher energy levels generates electron-hole pairs. The electrons (e^-) and holes (h^+) generated via light are subsequently engaged in oxidation-reduction processes with adsorbed substances on the surface of the NiO catalyst. The photogenerated electrons (e^-) in the conduction band of NiO can react with adsorbed species, typically oxygen molecules (O_2), water (H_2O), or organic molecules, leading to reduction reactions, such as the conversion of O_2 to superoxide radicals (O^{2-}) or the reduction of organic pollutants to less harmful substances (Duan *et al,* 2022). Photogenerated holes (h^+) in the valence band of NiO can oxidize water molecules (H_2O) or hydroxide ions (OH^-) adsorbed on the surface, generating hydroxyl radicals (OH*) or oxygen gas (O_2). These radicals are highly reactive and can oxidize organic pollutants (BB and CV dye) molecules through weak van der Waals forces or electrostatic interactions into smaller, less harmful molecules (Khattab *et al,* 2022).

Figure 15. Dye degradation mechanism of prepared nanoparticle and nanocomposite

Adding Polypyrrole polymer to the NiO matrix enhances the segregation of photogenerated electron-hole pairs. When light is absorbed, electrons are quickly transferred from the NiO to the polymer, preventing recombination with holes and thus increasing the efficiency of the photocatalytic process . The polypyrrole provides improved charge transfer and conductivity, while NiO offers catalytic activity and stability. Thus, the NiO-PPy nanocomposite enhances the photocatalytic activity compared to pure NiO nanoparticles.

4. Conclusion

The study on NiO-PPy nanocomposites synthesized via hydrothermal methods using Eucalyptus leaf extracts highlights their significant potential in environmental remediation

applications. The structural analysis confirmed the formation of highly crystalline NiO with a cubic structure and exhibited a crystalline nature with increased crystallite size corresponding to higher concentrations of polypyrrole. The FTIR spectra confirmed the presence of key functional groups, illustrating strong interactions between the NiO nanoparticles and the polypyrrole polymer while the inclusion of polypyrrole enhanced the composite's optical and morphological properties and contributed to the composite's enhanced properties. The nanocomposites exhibited remarkable photocatalytic efficiency, particularly in degrading the anionic Brilliant blue dye under sunlight, achieving nearly 97% degradation. The degradation kinetics followed a pseudo-first-order model, indicating that the photocatalytic process is highly effective. Moreover, the stability of the NiO-PPy nanocomposites was tested over five cycles, demonstrating consistent performance with negligible loss in degradation efficiency. This stability highlights the potential for practical applications in wastewater treatment and environmental remediation.

References

Aldhaher A., Rabiee N. and Iravani S. (2024). Exploring the synergistic potential of MXene-MOF hybrid composites: A perspective on synthesis, properties, and applications, *Hybrid Advances*, **5**, 100131.

Bin S., Norrman K. and Abdulhamid M.A. (2024). Thermal transformation of date seeds from nonporous to porous materials: Insights on structural changes using chemical and physical characterization, *Journal of Analytical and Applied Pyrolysis*, **177**, 106353.

Bones D.L., Daly S.M., Mangan T.P. and Plane J.M.C. (2020). A study of the reactions of Ni+ and NiO^+ ions relevant to planetary upper atmospheres, *Physical Chemistry Chemical Physics*, **22**, 8940–8951.

Deng Y., Shi Y. and Li L. (2024). Molecular modification: A promising strategy for the design of donor-acceptor-type organic polymers photocatalyst, *Applied Catalysis B: Environment and Energy*, **352**, 124043.

Du X., Heumueller T. and Gruber W. (2020). Unraveling the microstructure-related device stability for polymer solar cells based on nonfullerene small-molecular acceptors, *Advanced Materials*, **32**, 1908305.

Duan S., Wu R. and Xiong Y.H (2022). Multifunctional antimicrobial materials: From rational design to biomedical applications, *Progress in Materials Science,* **125**, 100887.

Idumah C.I. and Obele C.M. (2021). Understanding interfacial influence on properties of polymer nanocomposites, *Surfaces and Interfaces*, **22**, 100879.

Khattab T.A., Abdelrahman M.S. and Rehan M. (2020). Textile dyeing industry: environmental impacts and remediation, *Environmental Science and Pollution Research*, **27**, 3803–3818.

Liu W., Wang S. and Wang J. (2022). Supercritical hydrothermal synthesis of nano-zinc oxide: Process and mechanism, *Ceramics International*, **48**, 22629–22646.

Liu X., Zheng W. and Kumar R. (2022). Conducting polymer-based nanostructures for gas sensors, *Coordination Chemistry Reviews*, **462**, 214517.

Lv X., Zhang J. and Dong X. (2020). Layered double hydroxide nanosheets as efficient photocatalysts for NO removal: Band structure engineering and surface hydroxyl ions activation, *Applied Catalysis B: Environment and Energy*, **277**, 119200.

Pandey A., Dalal S., Dutta S. and Dixit A. (2021). Structural characterization of polycrystalline thin films by X-ray diffraction techniques, *Journal of Materials Science: Materials in Electronics*, **32**, 1341–1368.

Peng Y., Bian Z. and Wang F. (2024). Electrocatalytic degradation of p-nitrophenol on metal-free cathode: Superoxide radical (O^{2-}) production via molecular oxygen activation, *Journal of Hazardous Materials*, **462**, 132797.

Restrepo C.V. and Villa C.C. (2021). Synthesis of silver nanoparticles, influence of capping agents, and dependence on size and shape: A review, *Environmental Nanotechnology, Monitoring & Management*, **15**, 100428.

Tian Y., He C. and He L.(2024). Doping heteroatoms to form multiple hydrogen bond sites for enhanced interfacial reconstruction and separations, *Journal of Hazardous Materials*, **472**, 134477.

Walkinshaw C., Lindeque P.K. and Thompson R. (2020). Microplastics and seafood: lower trophic organisms at highest risk of contamination, *Ecotoxicology and Environmental Safety*, **190**, 110066.

Yan J., Huang Y. and Liu X. (2021). Polypyrrole-Based Composite Materials for Electromagnetic Wave Absorption, *Polymer Reviews*, **61**, 646–687.

Yan Y., Yang G. and Xu J.L. (2021). Conducting polymer-inorganic nanocomposite-based gas sensors: a review, *Science and Technology of Advanced Materials,* **21**, 768–786.

Zhao C., Zhang W. and Zhang Y. (2024). Influence of multivalent background ions competition adsorption on the adsorption behavior of azo dye molecules and removal mechanism: Based on machine learning, DFT and experiments, *Separation and Purification Technology*, **341**, 126810.

Zheng B., Fan J. and Chen B. (2022). Rare-Earth Doping in Nanostructured Inorganic Materials, *Chemical Reviews*, **122**, 5519–5603.